International Journal of Mass Spectrometry 309 (2012) 30–38

Contents lists available at SciVerse ScienceDirect

International Journal of Mass Spectrometry

journal homepage: www.elsevier.com/locate/ijms

On the phase dependence of the interconversion of the motional modes in a Penning trap by quadrupolar excitation

Martin Kretzschmar*

Institut für Physik, Johannes Gutenberg-Universität, 55099 Mainz, Germany

ARTICLE INFO

Article history:
Received 29 April 2011
Received in revised form 20 August 2011
Accepted 20 August 2011
Available online 9 September 2011

PACS:
37.10.Ty (ion traps)
82.80.Qx (ion cyclotron resonance mass spectrometry)
82.80.Rt (time-of-flight mass spectrometry)

Keywords:
Mass spectrometry
Ion motion
Ion cyclotron resonance
Interconversion of motional modes
Quadrupole excitation
Ramsey excitation

ABSTRACT

The interconversion of the radial motional modes in a Penning trap (magnetron and cyclotron modes) by an external quadrupolar rf-field with a frequency near the true cyclotron frequency ω_c plays an important role in the measurement cycle of Penning trap mass spectrometry. Ions to be measured are prepared in a state of magnetron motion which is then resonantly converted into cyclotron motion. The data analysis is usually carried out under the assumption that the initial motional state of the ions has been a pure magnetron state. In reality, however, a small component of cyclotron motion is always present in the ion's initial motional state. This component introduces a dependence on the initial phases of the quadrupolar rf-field and of the magnetron and cyclotron oscillators. This paper explores how excitation curves, conversion times and conversion line shapes depend on these phases and on the initial radius of the cyclotron motion. Since most experiments cannot control all of these phases the data must be interpreted in terms of phase-averaged quantities. These are slightly more general than those for pure magnetron motion. Most importantly, there are no shifts of the maxima and minima of phase-averaged conversion profiles compared to those predicted with pure magnetron motion in the initial state, so that the mass determinations are not affected. The theory predicts experimental data points to fall not on a mathematical curve, as for pure magnetron motion in the initial state, but within bands about the phase-averaged curves, with a finite width roughly proportional to the radius of the initial cyclotron motion. The scattering of data points can give rise to a loss of contrast of measured conversion line shapes. The component of cyclotron motion in the initial state introduces an additional parameter into the analytical expressions for conventional and Ramsey type excitation that could in some cases be useful for data fitting.

1. Introduction

In recent years Penning traps have developed into important tools for high-precision mass spectrometry on charged particles [1,2]. Penning traps confine charged particles by means of a static electric quadrupole field and a strong homogeneous magnetic field B, the ion motion in the trap is characterized by three oscillator frequencies, the axial frequency ω_z, the modified cyclotron frequency ω_+, and the magnetron frequency ω_- [3–5]. The mass m of a particle with electric charge q is determined by a precise measurement of the 'true' cyclotron frequency, $\omega_c = qB/m$. For the ideal hyperbolic Penning trap we have $\omega_+ + \omega_- = \omega_c$.

For a mass determination one collects the results of measurements performed on several hundreds of single ions. Commonly the first step is the insertion of the ions near the trap center, followed by an enlargement of their magnetron radius to a desired initial value $R_-(0)$ by means of a pulse of dipolar rf-radiation with the frequency of the magnetron oscillator [6,7]. Alternatively the ion injection can be performed by the more recent "Lorentz steerer" technique [8]. In either case ideally one aims at preparing the ions in a state of pure magnetron motion (*i.e.*, with initial cyclotron radius $R_+(0) = 0$), but practically a small component of cyclotron motion will always be left, $R_-(0) \gg R_+(0) > 0$. Subsequently an azimuthal electric quadrupole field with a frequency ω_q close to the cyclotron frequency ω_c is applied. At the resonance, *i.e.*, for $\omega_q \approx \omega_c$ the magnetron motional mode is converted into the cyclotron motional mode [6,9,10]. Full conversion takes place for the proper product of excitation time and amplitude of the quadrupolar field. A frequency scan exhibits a resonance peak at the true cyclotron frequency ω_c. A time-of-flight technique (TOF-ICR) [11] is used for the detection of the ions. For more details see *e.g.*, [12].

The resonant conversion of an ion's magnetron motion into cyclotron motion by a pulse of external quadrupolar rf-radiation is the crucial step in the measurement procedure. Experimental data are usually compared to theoretical curves that are deduced from the assumption of pure magnetron motion in the initial state.

* Tel.: +49 6131 477234
E-mail address: Martin.Kretzschmar@uni-mainz.de

1387-3806/$ – see front matter © 2011 Elsevier B.V. All rights reserved.
doi:10.1016/j.ijms.2011.08.022

In this case the phases of the radiation field and of the magnetron and cyclotron oscillators drop out from all mathematical expressions.

In practice it is unavoidable that a small component of cyclotron motion has survived the preparation of the initial state. All results then depend on the initial value of the radius $R_+(0)$ of the cyclotron motion and on a specific combination of the above mentioned phases. This study investigates manifestations and consequences of this fact for conventional one-pulse quadrupolar excitation and for two-pulse Ramsey excitation. We find that conversion line shapes are phase dependent and are in general asymmetric with respect to the central peak. The position of the central peak is shifted, dependent on the phase, by small amounts away from the cyclotron frequency ω_c. Since most experiments cannot control the phase of the cyclotron motion their theoretical interpretation requires an average over this phase and over the probability distribution of the initial radius $R_+(0)$. Fortunately, the central peak of the averaged conversion line shape occurs exactly at the cyclotron frequency ω_c, so that mass determinations are not adversely affected. The averaged line shape is symmetric with respect to the central peak, and for both one-pulse and two-pulse excitation a generalized formula relates the averaged conversion line shape to the conventional formulas for an initial pure magnetron motional state (see Eqs. (30) and (41) below). These formulas offer the expectation value $\langle R_+^2(0)\rangle$ as a possible new parameter for data fitting. Another consequence of the phase dependence is the fact that experimental data points are predicted to fall into bands of finite width about the phase-averaged conversion profiles, so that data plots have a somewhat diffuse appearance. The width of these bands is to lowest order proportional to $R_+(0)$. Cooling the cyclotron motion in the initial state can therefore be essential for obtaining well-defined and precise conversion profiles.

This paper also serves as a preparatory study for a major theoretical investigation of the interconversion of the motional modes by external octupolar rf-fields, to be reported in future publications. In this case analogous questions must be answered, but in a more complicated non-linear setting. With a similar motivation Ringle et al. [14] have recently studied the phase-dependence of conversion by quadrupolar rf-fields by simulations and in experiments.

The plan of the paper is as follows: in the next section we sketch the theoretical concepts underlying our approach. Starting from quantum mechanical considerations we obtain an effective interaction between the external quadrupolar rf-field and the ion moving in the Penning trap that describes the conversion of excitation quanta of the magnetron oscillator into quanta of the cyclotron oscillator with conservation of the total number of quanta. The rigorous solution of the ensuing equations of motion yields the complex oscillator amplitudes for the cyclotron and the magnetron oscillators in closed analytical form. From these we obtain an expression for the function $n_+(t, \delta, \chi, g) = N_+(t)/N_{\mathrm{tot}}$ which tells us what fraction of all quanta in the system resides in the cyclotron oscillator, as a function of time t, detuning δ, phase χ, initial radius $R_+(0)$, and coupling parameter g. This function is the basis for all further discussion. Section 3 studies the excitation function, *i.e.*, the function n_+ with detuning $\delta = 0$. Sections 4 and 5 are devoted to the conversion line shapes for one-pulse and two-pulse excitation, respectively. Section 6 summarizes our conclusions.

2. Mathematical framework

The ion motion in an ideal hyperbolic Penning trap is described by three harmonic oscillators, denoted as cyclotron (+), magnetron (−), and axial (z) oscillators. The axial motion is of no importance for this paper, the corresponding term will be omitted in the following. In the quantum mechanical formalism of the Heisenberg picture the Hamiltonian for the two azimuthal modes is given as

$$H_0(t) = \hbar\omega_+ a_+^\dagger(t)\, a_+(t) - \hbar\omega_- a_-^\dagger(t)\, a_-(t), \tag{1}$$

where $\omega_k = 2\pi\nu_k$ is the oscillator frequency and where $a_k(t)$ and $a_k^\dagger(t)$ are annihilation and creation operators for the oscillator quanta ($k = +, -$).

An azimuthal quadrupolar rf-field acts on an ion in the Penning trap in various ways. Depending on the frequency three resonant cases can be distinguished: $\omega_q = 2\,\omega_+$, $\omega_q = 2\,\omega_-$, and $\omega_q = \omega_+ + \omega_-$ [13]. In the first case the rf-field amplifies or reduces the cyclotron motion without affecting the magnetron oscillator, in the second case it amplifies or reduces the magnetron motion without affecting the cyclotron oscillator, and in the third case the quadrupolar rf-field transfers excitation from the magnetron oscillator to the cyclotron oscillator, and vice versa. This case, known as the 'interconversion of oscillator modes', is the most important one and shall be considered exclusively in the following. The interaction of the ion with the quadrupolar rf-field is most clearly understood in the quantum mechanical formalism where one can decompose the interaction operator into a sum of terms for the processes mentioned [15]. By means of the 'rotating wave approximation' [16], limiting the frequency ω_q of the azimuthal quadrupolar rf-field to a band around the cyclotron frequency ω_c, the effective interaction for the interconversion of modes can be isolated as

$$H_1(t) = \hbar g(e^{-i\phi_q(t)} a_+^\dagger(t) a_-(t) + e^{+i\phi_q(t)} a_-^\dagger(t) a_+(t)), \tag{2}$$

where g is a coupling parameter with the dimension of a frequency and proportional to the amplitude of the quadrupolar rf-field, and where $\phi_q(t) = \omega_q t + \chi_q$ is the phase of the quadrupolar rf-field at time t, with $\chi_q = \phi_q(0)$. This interaction has the remarkable property that for each oscillator quantum that is annihilated a quantum of the other oscillator is created, and vice versa. Thus the total number of oscillator quanta in the system is conserved and is defined by the starting values of the system at $t = 0$:

$$N_{\mathrm{tot}} = N_+(0) + N_-(0) \;=\; N_+(t) + N_-(t) = a_+^\dagger(t)\, a_+(t) + a_-^\dagger(t)\, a_-(t). \tag{3}$$

The total Hamiltonian is $H(t) = H_0(t) + H_1(t)$. It yields Heisenberg equations of motion for the annihilation operators $a_\pm(t)$ and the creation operators $a_\pm^\dagger(t)$ that can be solved exactly [15,19]:

$$\frac{\mathrm{d}}{\mathrm{d}t} a_+(t) = -i\omega_+ a_+(t) - ige^{-i\phi_d(t)} a_-(t), \tag{4}$$

$$\frac{\mathrm{d}}{\mathrm{d}t} a_-(t) = +i\omega_- a_-(t) - ige^{+i\phi_d(t)} a_+(t). \tag{5}$$

Equations for the creation operators are obtained by taking the adjoints of these equations.

The quantum mechanical considerations serve to justify the effective interaction, Eq. (2), and the conservation law for the total number of quanta in the system, Eq. (3). From here on it is sufficient to treat the ion motion in the Penning trap as a classical problem. The transition to a classical description uses expectation values of the quantum mechanical annihilation operators for 'quasi-classical states', also known as 'minimum uncertainty coherent oscillator states' $|\alpha\rangle$, where α is a complex number [16]. These expectation values yield complex oscillator amplitudes $\alpha_\pm(t)$ that can be considered as classical quantities and that shall be in the following the basic physical quantities for our discussion, ([15] and Section 2.4 of [19].

$$\alpha_\pm(t) = \langle\alpha|a_\pm(t)|\alpha\rangle, \qquad \alpha_\pm^*(t) = \langle\alpha|a_\pm^\dagger(t)|\alpha\rangle. \tag{6}$$

The asterisk means complex conjugation. The Heisenberg equations of motion for the annihilation operators $a_\pm(t)$ (4), (5) translate

into first order differential equations for the complex oscillator amplitudes $\alpha_\pm(t)$ with the solution (see [19], Eqs. (46) and (47))

$$\alpha_+(t) = e^{-i(\omega_+ + \delta/2)t}\left[\left(\cos\frac{\omega_R t}{2} + i\frac{\delta}{\omega_R}\sin\frac{\omega_R t}{2}\right)\alpha_+(0) - i\frac{2g}{\omega_R}\sin\frac{\omega_R t}{2}e^{-i\chi_q}\alpha_-(0)\right], \tag{7}$$

$$\alpha_-(t) = e^{+i(\omega_- + \delta/2)t}\left[-i\frac{2g}{\omega_R}\sin\frac{\omega_R t}{2}e^{+i\chi_q}\alpha_+(0) + \left(\cos\frac{\omega_R t}{2} - i\frac{\delta}{\omega_R}\sin\frac{\omega_R t}{2}\right)\alpha_-(0)\right]. \tag{8}$$

Here $\delta = \omega_q - \omega_c$ denotes the detuning of the quadrupolar rf-field, and $\omega_R = \sqrt{4g^2 + \delta^2}$ is the Rabi frequency of the interconversion. Thus the time development of the complex oscillator amplitudes is described, up to phase factors by the unitary matrix

$$\mathcal{M}'(t;\delta,g) = \begin{pmatrix} \cos\left(\frac{\omega_R t}{2}\right) + i\frac{\delta}{\omega_R}\sin\left(\frac{\omega_R t}{2}\right) & -i\frac{2g}{\omega_R}\cdot\sin\left(\frac{\omega_R t}{2}\right) \\ -i\frac{2g}{\omega_R}\cdot\sin\left(\frac{\omega_R t}{2}\right) & \cos\left(\frac{\omega_R t}{2}\right) - i\frac{\delta}{\omega_R}\sin\left(\frac{\omega_R t}{2}\right) \end{pmatrix}. \tag{9}$$

The initial values of the complex oscillator amplitudes $\alpha_\pm(0)$ are factorized into a modulus and a phase factor,

$$\alpha_+(0) = |\alpha_+(0)|\, e^{-i\chi_+}, \tag{10}$$

$$\alpha_-(0) = |\alpha_-(0)|\, e^{+i\chi_-}. \tag{11}$$

We then deduce from Eqs. (7) and (8)

$$|\alpha_+(t)|^2 = |(\mathcal{M}'_{11}\cdot|\alpha_+(0)| + e^{-i\chi}\mathcal{M}'_{12}\cdot|\alpha_-(0)|)|^2, \tag{12}$$

$$|\alpha_-(t)|^2 = |(e^{+i\chi}\mathcal{M}'_{21}\cdot|\alpha_+(0)| + \mathcal{M}'_{22}\cdot|\alpha_-(0)|)|^2, \tag{13}$$

with $\chi = \chi_q - \chi_+ - \chi_-$. The initial phases always occur in this combination.

For the practical application of these results it is useful to know that the instantaneous radii for the cyclotron and the magnetron motion are given by

$$R_+(t) = \sqrt{\frac{2\hbar}{m\omega_1}}|\alpha_+(t)|, \quad R_-(t) = \sqrt{\frac{2\hbar}{m\omega_1}}|\alpha_-(t)|, \tag{14}$$

with $\omega_1 = \omega_+ - \omega_- = \sqrt{\omega_c^2 - 2\,\omega_z^2}$. The expectation value of Eq. (3) then becomes

$$\langle N_{\mathrm{tot}}\rangle = \alpha_+^*(t)\alpha_+(t) + \alpha_-^*(t)\alpha_-(t) = \frac{m\omega_1}{2\hbar}\left(R_+^2(t) + R_-^2(t)\right). \tag{15}$$

For the study of the interconversion of modes the main interest is in the fractions $n_\pm$ of oscillator quanta that are residing in the cyclotron and magnetron oscillators, respectively. These can now be expressed as

$$n_\pm(t) = \frac{\langle N_\pm(t)\rangle}{\langle N_{\mathrm{tot}}\rangle} = \frac{|\alpha_\pm(t)|^2}{|\alpha_+(0)|^2 + |\alpha_-(0)|^2} = \frac{R_\pm^2(t)}{R_+^2(0) + R_-^2(0)}. \tag{16}$$

We observe $n_+(t) + n_-(t) = 1$. The initial values are

$$n_{0\pm} = n_\pm(0) = \frac{R_\pm^2(0)}{R_+^2(0) + R_-^2(0)}. \tag{17}$$

The time development of the fractions $n_\pm(t)$ can now be described in terms of closed analytical expressions which are the basis of all discussions in the following sections. For clarity we also display the parameters δ, χ, and g on which these expressions depend:

$$n_+(t,\delta,\chi,g) = \left|\left(\cos\left(\frac{\omega_R t}{2}\right) + i\frac{\delta}{\omega_R}\sin\left(\frac{\omega_R t}{2}\right)\right)\cdot\sqrt{n_{0+}} - i\,e^{-i\chi}\frac{2g}{\omega_R}\cdot\sin\left(\frac{\omega_R t}{2}\right)\cdot\sqrt{n_{0-}}\right|^2, \tag{18}$$

$$n_-(t,\delta,\chi,g) = \left|-i\,e^{+i\chi}\frac{2g}{\omega_R}\cdot\sin\left(\frac{\omega_R t}{2}\right)\cdot\sqrt{n_{0+}} + \left(\cos\left(\frac{\omega_R t}{2}\right) + i\frac{\delta}{\omega_R}\sin\left(\frac{\omega_R t}{2}\right)\right)\cdot\sqrt{n_{0-}}\right|^2. \tag{19}$$

For theoretical discussions the use of the dimensionless variables $\theta = (2g/\pi)\cdot t$ and $\eta = \delta/(2g)$ offers great advantages. Therefore we display the fractions $n_\pm$ also in the dimensionless formulation:

$$n_+(\theta,\eta,\chi) = n_{0+} + \frac{1}{1+\eta^2}\sin^2\left(\sqrt{1+\eta^2}\theta\frac{\pi}{2}\right)(1-2\,n_{0+}) - \left[\sin\chi\,\frac{1}{\sqrt{1+\eta^2}}\sin\left(\sqrt{1+\eta^2}\theta\pi\right) + \cos\chi\,\frac{\eta}{1+\eta^2}\sin^2\left(\sqrt{1+\eta^2}\theta\frac{\pi}{2}\right)\right]\cdot\sqrt{n_{0+}n_{0-}}, \tag{20}$$

$$n_-(\theta,\eta,\chi) = 1 - n_+(\theta,\eta,\chi). \tag{21}$$

We note that the last term in Eq. (20) is an odd function of η, *i.e.*, it changes sign under the substitution $\eta \leftrightarrow -\eta$. It is thus responsible for asymmetric conversion line shapes, as discussed in detail below. Similarly the second term is an odd function of χ and changes sign under the substitution $\chi \leftrightarrow -\chi$, thus preventing symmetry under this exchange. Finally, integrating both sides of Eq. (20) over χ we see that the first term represents the phase-averaged function $\overline{n}_+(\theta,\eta) = (2\pi)^{-1}\int_{-\pi}^{+\pi}\mathrm{d}\chi\cdot n_+(\theta,\eta,\chi)$.

3. One-pulse excitation functions

We begin our study of the interconversion of the motional modes by considering the special case that the quadrupolar radiation has a frequency exactly equal to the true cyclotron frequency, $\omega_q = \omega_c$, or equivalently $\delta = 0$. Then we denote the functions $n_\pm(t, \delta, \chi)|_{\delta=0}$ as 'excitation functions' for the respective mode. Excitation functions describe the progress of the conversion process after the quadrupolar rf-field with the exact resonance frequency ω_c has acted for a time interval τ. Our general expressions for the fractions $n_\pm$, Eqs. (18) and (19), reduce for $\delta = 0$ to

$$n_+(\tau,\delta=0,\chi,g) = \left|\cos(g\tau)\cdot\sqrt{n_{0+}} - i\,e^{-i\chi}\cdot\sin(g\tau)\cdot\sqrt{n_{0-}}\right|^2, \tag{22}$$

$$n_-(\tau,\delta=0,\chi,g) = \left|-i\,e^{+i\chi}\cdot\sin(g\tau)\cdot\sqrt{n_{0+}} + \cos(g\tau)\cdot\sqrt{n_{0-}}\right|^2, \tag{23}$$

or in dimensionless notation with $\eta = 0$

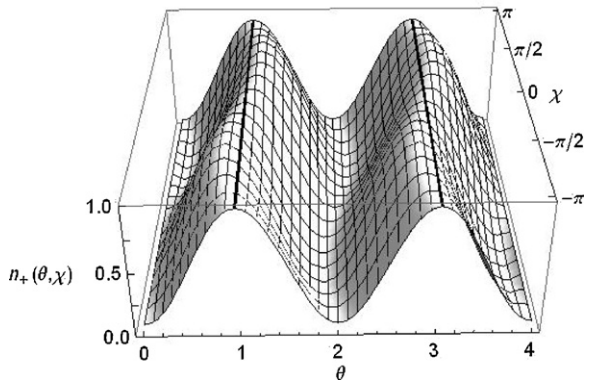

Fig. 1. Plot of the surface $n_+(\theta, \eta = 0, \chi)$ over two Rabi periods ($0 \le \theta \le 4$) and over $-\pi \le \chi \le +\pi$. Cuts along lines of constant phase χ represent excitation functions for the cyclotron mode with phase χ as function of the dimensionless time θ. The thick black lines are at $\theta = 1$ and at $\theta = 3$. We observe positive or negative delays $\theta_0(\chi)$ of the conversion maxima depending on whether $0 < \chi < \pi$ or $-\pi < \chi < 0$. The figure was calculated with $R_+(0) = 0.25\, R_-(0)$.

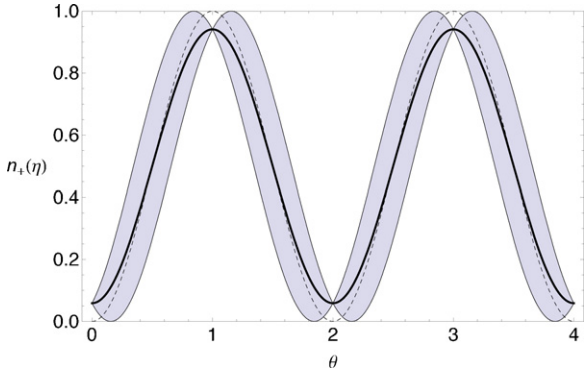

Fig. 2. Projecting Fig. 1 into two dimensions the phase-dependent excitation functions of the cyclotron mode fill the shaded areas. The phase-averaged excitation function, Eq. (29), is represented by the solid black line. The dashed line is the excitation function for a state of initially pure magnetron motion. The figure was calculated with $R_+(0) = 0.25\, R_-(0)$.

$$n_+(\theta, \eta = 0, \chi) = n_{0+} + \sin^2\left(\theta\frac{\pi}{2}\right)(1 - 2\,n_{0+}) - \sin\chi\,\sin\left(\theta\pi\right) \cdot \sqrt{n_{0+}n_{0-}}, \tag{24}$$

$$n_-(\theta, \eta = 0, \chi) = 1 - n_+(\theta, \eta = 0, \chi). \tag{25}$$

Maxima and minima of the function $n_+(\theta, \eta = 0, \chi)$ are characterized by the condition

$$\frac{\mathrm{d}}{\mathrm{d}\theta} n_+(\theta, \eta = 0, \chi) = (\pi/2)\sin(\theta\pi)\,(1 - 2\,n_{0+}) - \pi\cos(\theta\pi)\,\sin\chi \cdot \sqrt{n_{0+}n_{0-}} = 0. \tag{26}$$

If the initial state is a pure magnetron state then $n_{0-} = 1$ and $n_+ = 0$, so that $n_+(\theta, \eta = 0, \chi) = \sin^2(\theta\pi)$. We have a Rabi oscillation with period 2, complete conversion of the initial magnetron state into a pure cyclotron state for $\theta = 1, 3, 5, \ldots$ and complete reconversion into a pure magnetron state for $\theta = 2, 4, 6, \ldots$. Therefore the time unit $\theta = 1$ or equivalently $\tau_c = \pi/(2g)$ is denoted as 'conversion time'. In the general case, when $n_{0+} \neq 0$, conversion maxima (k odd integer) and conversion minima (k even integer) are found at $\theta_k(\chi) = k + \theta_0(\chi)$, where

$$\theta_0(\chi) = \frac{1}{\pi}\,\arctan\left(2\sin\chi \cdot \frac{\sqrt{n_{0+}n_{0-}}}{n_{0-} - n_{0+}}\right), \tag{27}$$

is a delay relative to the case with initially pure magnetron motion. The delay function $\theta_0(\chi)$ depends on the phase χ and on the initial fraction n_{0+} of cyclotron motion. Assuming $n_{0+} \ll n_{0-}$ we have

$$\theta_0(\chi) \approx \frac{1}{\pi}\,\arctan\left(2\sin\chi \cdot \frac{R_+(0)}{R_-(0)}\right) \approx \frac{1}{\pi}\left(2\sin\chi \cdot \frac{R_+(0)}{R_-(0)} - \frac{1}{3}\left(2\sin\chi \cdot \frac{R_+(0)}{R_-(0)}\right)^3 + \ldots\right). \tag{28}$$

In leading approximation the delay is proportional to the ratio $R_+(0)/R_-(0)$.

In Fig. 1 the delay function $\theta_0(\chi)$ has been illustrated by plotting the surface $n_+(\theta, \eta = 0, \chi)$ over the (θ, χ)-plane. Cuts along the lines of constant χ represent the excitation function for that value of the phase. We see that the delay $\theta_0(\chi)$ is positive for $0 < \chi < \pi$ and negative for $-\pi < \chi < 0$. For $0 < \chi < \pi$ the conversion process starts with the conversion of the initial component of cyclotron motion into magnetron motion, thus causing a positive delay, then the conversion of magnetron into cyclotron motion sets in. For $-\pi < \chi < 0$ the conversion of magnetron into cyclotron motion starts immediately, thus we have a negative delay. By projection of Fig. 1 along the χ-axis onto the (θ, n_+)-plane we obtain Fig. 2 showing the phase-averaged excitation function (solid line)

$$\overline{n}_+(\theta) = n_{0+} + \sin^2\left(\theta\pi/2\right)(1 - 2\,n_{0+}) \tag{29}$$

embedded into a shaded band that is generated by the excitation functions for given values of χ, where $-\pi \le \chi \le +\pi$. The width of the band is determined by the maximum and minimum delay.

These figures have been calculated, like most other figures of this paper, with an initial cyclotron radius $R_+(0) = \kappa\, R_-(0)$ with $\kappa = 0.25$. This rather large value was chosen to highlight the effects due to a cyclotron component in the initial state. Although most authors are not very specific about this detail of their experiments one may expect that they prepare the initial state with a smaller component of cyclotron motion. In a paper by Eliseev et al. [17] these authors estimate $\kappa = 0.14$.

Finally we note that the average of the delay function $\theta_0(\chi)$ over all phases $-\pi \le \chi \le +\pi$ vanishes, independently of the ratio $\kappa = R_+(0)/R_-(0)$. Therefore the phase-averaged conversion time is $\theta = 1$, equivalent to $\tau_c = \pi/(2g)$ as in the case of initially pure magnetron motion. Thus it seems reasonable to choose this pulse duration also for our study of 1-pulse conversion line shapes in the next section.

4. Conversion line shapes for 1-pulse excitation

Conversion profiles for 1-pulse excitation have been discussed extensively by König et al. [18]. They pointed out the relevance of the phase combination $\chi = \chi_q - \chi_+ - \chi_-$, but did not explore the phase dependence of conversion profiles in any detail. Recently Ringle et al. [14] noticed that, depending on the value of χ, conversion profiles can become asymmetric. They supported this insight by simulations and experiments.

We shall discuss conversion line shapes for a pulse duration $\theta = 1$, equal to the phase-averaged conversion time. This guarantees that after taking the average over the phase the maximal degree of conversion is achieved. Keeping the phase χ fixed and inserting $\theta = 1$ into Eq. (20) we obtain the function $n_+(\theta = 1, \eta, \chi = \text{const})$ that describes the conversion result as a function of the detuning parameter η when the phase has a given value χ.

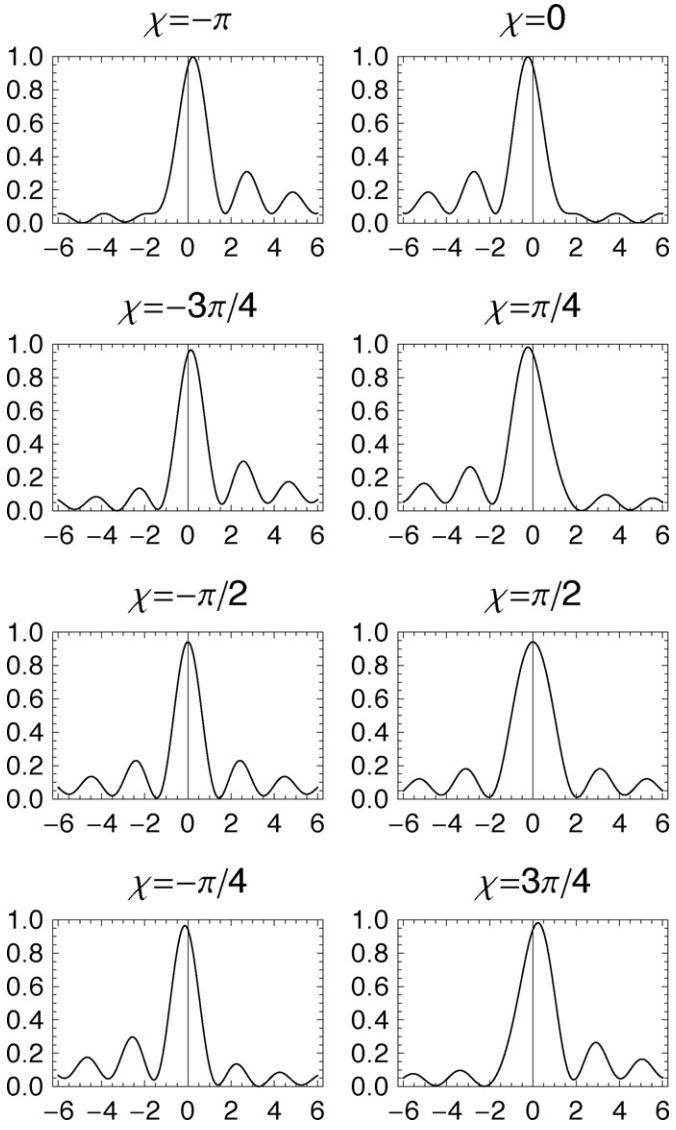

Fig. 3. The figure shows conversion line shapes for conventional 1-pulse quadrupole excitation for various values of the phase χ, calculated with a ratio of initial radii $\kappa \approx 0.25 R_+(0)/R_-(0)$. The curves are plots of $n_+(\theta = 1, \eta, \chi = \text{const})$ as a function of the detuning parameter η.

Fig. 3 shows conversion line shapes for different values of χ. Note that the line shapes are in general not symmetric under the substitution $\eta \to -\eta$. According to (20) such symmetry is obtained only for $\chi = \pm\pi/2$, *i.e.*, $\cos\chi = 0$. Maximal asymmetry is found for $\chi = 0, \pm\pi$, *i.e.*, $\sin\chi = 0$. Due to the asymmetry the peak conversion does not occur exactly at the cyclotron frequency ω_c (*i.e.*, $\eta = 0$), but with some small detuning $\eta_a = \delta_a/(2g) \neq 0$ that is proportional to the initial cyclotron radius $R_+(0)$. This is visible in Fig. 3, but much more clearly in Fig. 4.

It is of great interest to estimate the maximal shift of the peak conversion. The shifted peak position is obtained by evaluating the condition $(\mathrm{d}/\mathrm{d}\eta) n_+(\theta, \eta, \chi)|_{\theta=1, \chi=0 \text{ or } \pi} = 0$ in the regime of $\eta \ll 1$ and $\kappa = R_+(0)/R_-(0) \ll 1$. The result is $\eta_a \approx \kappa/(2(1-\kappa^2))$. The relative frequency shift follows from $\delta_a/\omega_c = \eta_a \cdot (2g/\omega_c)$. Remember that at resonance $2g$ is the Rabi frequency for interconversion, $2g = \omega_R = 2\pi\,\nu_R = 2\pi/(2\tau_c)$. Fortunately, thanks to the simple structure of Eq. (20) the asymmetries cancel out when we take the

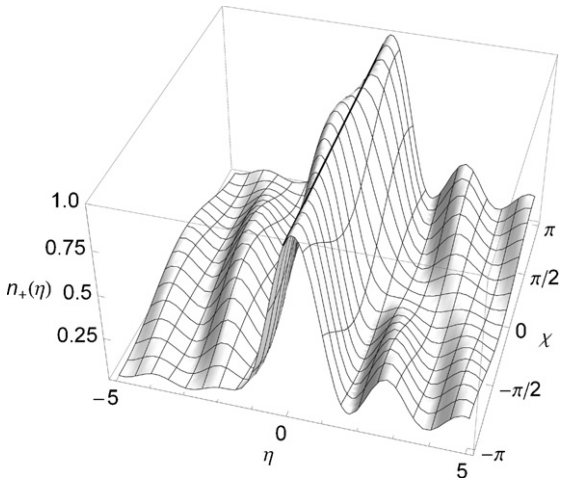

Fig. 4. The central peak for 1-pulse excitation coincides with the exact resonance position $\eta = 0$, marked by the heavy black line, only for phase $\chi = \pm\pi/2$, otherwise small shifts of the peak values toward both sides are observed. The figure shows a plot of the surface $n_+(\theta = 1, \eta, \chi)$, assuming $R_+(0) = 0.25\,R_-(0)$.

average over all phases. By averaging over the phase χ the right hand side of (20) simplifies to

$$\overline{n}_+(\eta) = n_{0+} + \frac{1}{1+\eta^2} \sin^2\left(\sqrt{1+\eta^2}\,\frac{\pi}{2}\right)(1 - 2\,n_{0+}). \tag{30}$$

When drawn in the same plot the set of all conversion profiles for $-\pi \le \chi \le -\pi$ fills the shaded region shown in Fig. 5. The central peak is represented by a band with a finite width that is determined by the initial radius of the cyclotron motion $R_+(0)$. The width is governed by η_a, the maximum shift of the central peak. The width of the band shrinks to zero when $\kappa = R_+(0)/R_-(0) \to 0$, *i.e.*, when the initial state is pure magnetron motion. The phase-averaged conversion profile, Eq. (30), is represented by the thick red line.

The foregoing discussions have assumed a given non-vanishing initial value of the radius of the cyclotron motion. Of course, such initial values are not only unknown in practice, they are also distributed over a certain range in a manner that depends on the preparation of the initial state. Thus the situation will differ from one experiment to the next. For definiteness let us therefore assume a Gaussian distribution for $R_+(0)$ with a variance $\sqrt{\langle R_+(0)^2\rangle} = \kappa\,R_-(0)$, and in addition a random distribution of the phase χ. We can then simulate for a sample of N single ions the expected outcome of an experiment. A simulation of data obtained by measuring

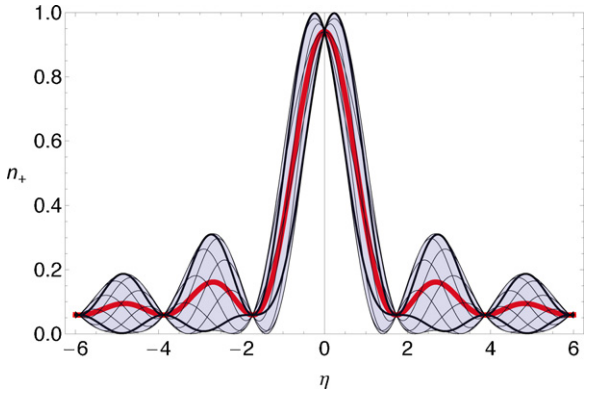

Fig. 5. The conversion profiles for fixed phase χ (Fig. 3) are here plotted in a single diagram. They fill the shaded region. The central resonance peak is defined not by single curve, but by a band of finite width which is determined by the initial radius of the cyclotron motion $R_+(0)$. This figure assumes $R_+(0) \approx 0.25 R_-(0)$. The thick red curve is the phase-averaged 1-pulse conversion profile, Eq. (30).

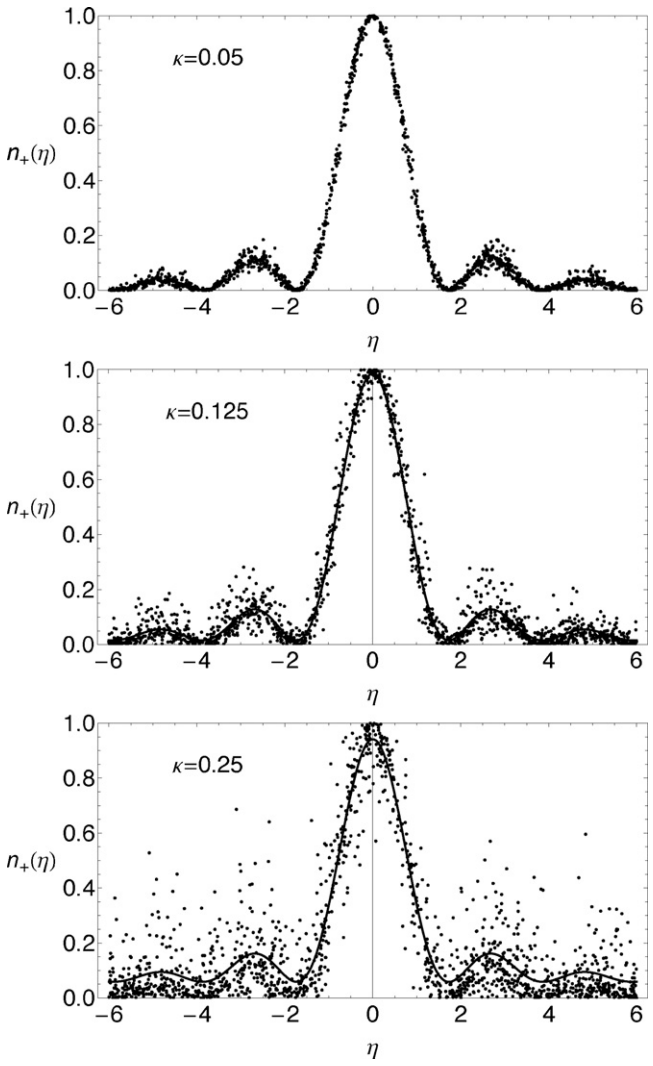

Fig. 6. Ion cyclotron resonances obtained by simulation of the conversion data of 1500 single ions, assuming random distribution of the phase χ and a Gaussian distribution for the initial value of the cyclotron radius $R_+(0)$. The three graphs show the progressive deterioration of the resonance signal as the variance of the Gaussian distribution is increased from $\kappa = 0.05$ to $\kappa = 0.25$. The black curve represents the phase-averaged conversion profile for $R_+(0) = \kappa R_-(0)$, Eq. (30).

1500 single ions is shown in Fig. 6 for three different values of the variance of the Gaussian distributions of the initial cyclotron radius. One observes an increasing degradation of the resonance signal as the variance is varied from $\kappa = 0.05$ to $\kappa = 0.25$.

5. Conversion line shapes for 2-pulse Ramsey excitation

Some time ago Bollen et al. [21] have suggested to use Ramsey's method of separated oscillatory fields [20] in Penning trap mass spectrometry. This proposal has recently been implemented for practical use in experiments [19,22]. As expected the method has brought a considerable increase in precision [23,24] and is now established in many laboratories [25–29]. In the simplest version the quadrupole field is acting on a trapped ion with two radiation pulses of duration $\tau_1 = \tau_c/2 = \pi/(4g)$, which are separated by a waiting interval of duration τ_0. With sufficiently long waiting intervals the resonant conversion line shape becomes subdivided into a set of narrow 'Ramsey fringes', as one sees by comparison of Figs. 3 and 7.

The theoretical description of the Ramsey excitation procedure is obtained by applying our Eqs. (7), (8) successively to the three time intervals with durations τ_1, τ_0, and τ_1 (for details see [19]).

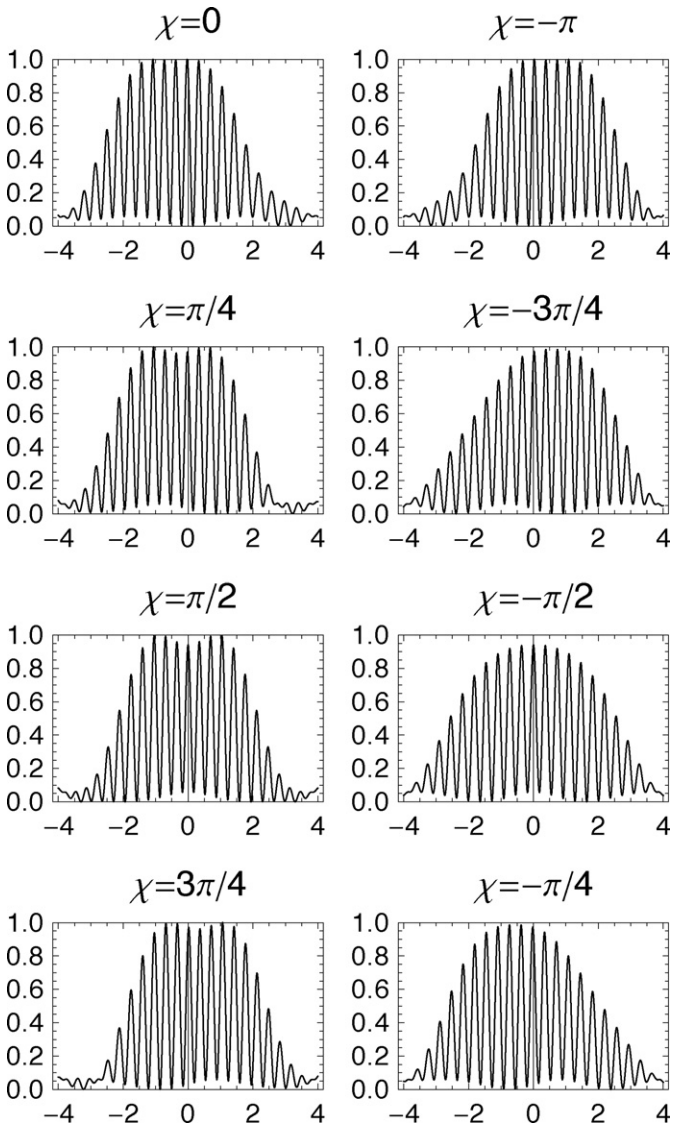

Fig. 7. The figure shows conversion line shapes for 2-pulse quadrupole excitation (Ramsey excitation) for various values of the phase χ. The curves are plots of $n_+(\theta_0 = 5, \theta_1 = 0.5, \eta, \chi = \text{const.})$ as a function of the detuning parameter η for given values of pulse duration (θ_1), waiting time (θ_0), and phase χ. For the initial radii we used $R_+(0) = 0.25\,R_-(0)$.

After completion of the Ramsey cycle the complex oscillator amplitudes are given by

$$\alpha_+(\tau_0 + 2\tau_1) = e^{-i(\omega_+ + \delta/2)(\tau_0 + 2\tau_1)} \times [\mathcal{R}'_{11}\,\alpha_+(0) + e^{-i\chi_q}\mathcal{R}'_{12}\,\alpha_-(0)], \tag{31}$$

$$\alpha_-(\tau_0 + 2\tau_1) = e^{+i(\omega_- + \delta/2)(\tau_0 + 2\tau_1)} \times [e^{+i\chi_q}\mathcal{R}'_{21}\,\alpha_+(0) + \mathcal{R}'_{22}\,\alpha_-(0)], \tag{32}$$

where the $\mathcal{R}'_{ik}$ are matrix elements of the 2×2 Ramsey matrix

$$\mathcal{R}'(\tau_0, \tau_1, \delta, g) = \begin{pmatrix} \mathcal{R}'_{11} & \mathcal{R}'_{12} \\ \mathcal{R}'_{21} & \mathcal{R}'_{22} \end{pmatrix} = \mathcal{M}'(\tau_1, \delta, g) \cdot \mathcal{M}'(\tau_0, \delta, 0) \cdot \mathcal{M}'(\tau_1, \delta, g). \tag{33}$$

As a product of three unitary matrices the Ramsey matrix $\mathcal{R}'$ is itself unitary. Working out the matrix elements we obtain

$$\begin{aligned}\mathcal{R}'_{11}(\tau_0,\tau_1,\delta,g) &= \mathcal{M}'_{11}(\tau_1,\delta,g)\mathcal{M}'_{11}(\tau_0,\delta,0)\mathcal{M}'_{11}(\tau_1,\delta,g)\\ &\quad+\mathcal{M}'_{12}(\tau_1,\delta,g)\mathcal{M}'_{22}(\tau_1,\delta,0)\mathcal{M}'_{21}(\tau_1,\delta,g)\\ &= \cos\frac{\delta\tau_0}{2}\left(\cos\omega_R\tau_1+i\frac{\delta}{\omega_R}\sin\omega_R\tau_1\right)\\ &\quad+i\sin\frac{\delta\tau_0}{2}\left[\frac{4g^2}{\omega_R^2}+\frac{\delta^2}{\omega_R^2}\cos\omega_R\tau_1+i\frac{\delta}{\omega_R}\sin\omega_R\tau_1\right],\end{aligned} \tag{34}$$

$$\begin{aligned}\mathcal{R}'_{12}(\tau_0,\tau_1,\delta,g) &= \mathcal{M}'_{11}(\tau_1,\delta,g)\mathcal{M}'_{11}(\tau_0,\delta,0)\mathcal{M}'_{12}(\tau_1,\delta,g)\\ &\quad+\mathcal{M}'_{12}(\tau_1,\delta,g)\mathcal{M}'_{22}(\tau_1,\delta,0)\mathcal{M}'_{22}(\tau_1,\delta,g)\\ &= -i\frac{2g}{\omega_R}\left[\cos\frac{\delta\tau_0}{2}\sin\omega_R\tau_1\right.\\ &\quad\left.+\frac{\delta}{\omega_R}\sin\frac{\delta\tau_0}{2}(\cos\omega_R\tau_1-1)\right],\end{aligned} \tag{35}$$

$$\mathcal{R}'_{21}(\tau_0,\tau_1,\delta,g)=\mathcal{R}'_{12}(\tau_0,\tau_1,\delta,g), \tag{36}$$

$$\mathcal{R}'_{22}(\tau_0,\tau_1,\delta,g)=\mathcal{R}'^{*}_{11}(\tau_0,\tau_1,\delta,g)=\mathcal{R}'_{11}(\tau_0,\tau_1,-\delta,g). \tag{37}$$

The asterisk in (37) denotes the complex conjugate.

From Eqs. (31) and (32) we can now obtain the fractions $n_{\pm}(\tau_0, \tau_1, \delta, g)$ of quanta in the cyclotron and magnetron oscillators, respectively,

$$n_+(\tau_0,\tau_1,\delta,\chi,g)=\left|\mathcal{R}'_{11}\sqrt{n_{0+}}+e^{-i\chi}\mathcal{R}'_{12}\sqrt{n_{0-}}\right|^2, \tag{38}$$

$$n_-(\tau_0,\tau_1,\delta,\chi,g)=\left|e^{+i\chi}\mathcal{R}'_{21}\sqrt{n_{0+}}+\mathcal{R}'_{22}\sqrt{n_{0-}}\right|^2, \tag{39}$$

with $\chi=\chi_q-\chi_+-\chi_-$. These equations are easily translated into representations in terms of the dimensionless variables $\theta=(2g/\pi)\tau$ and $\eta=\delta/(2g)$. When the initial state is a pure magnetron state ($n_{0+}=0$, $n_{0-}=1$) the dependence on the phase χ drops out and we find the well known result

$$\begin{aligned}n_+(\tau_0,\tau_1,\delta,g) &= \left|\mathcal{R}'_{12}(\tau_0,\tau_1,\delta,g)\right|^2\\ &= \frac{4g^2}{\omega_R^2}\left[\cos\frac{\delta\tau_0}{2}\sin\omega_R\tau_1+\frac{\delta}{\omega_R}\sin\frac{\delta\tau_0}{2}(\cos\omega_R\tau_1-1)\right]^2.\end{aligned} \tag{40}$$

As a first application let us consider Ramsey conversion profiles for various given values of the phase χ. To this end we first rewrite Eq. (38) in terms of $\theta_0=(2g/\pi)\tau_0$, $\theta_1=(2g/\pi)\tau_1$, and $\eta=\delta/(2g)$, thus obtaining $n_+(\theta_0, \theta_1, \eta, \chi)$. The choice $2\theta_1=1$ represents one half Rabi period and corresponds to a complete conversion of a pure magnetron state into a pure cyclotron state. The conversion profiles are plots of the fraction $n_+(\theta_0=\text{const}, \theta_1=0.5, \eta, \chi=\text{const})$ with the running variable η. In Fig. 7 we display eight such profiles for phases varying over the range $-\pi\le\chi\le+\pi$. The waiting time has been chosen to be $\theta_0=5$, corresponding to $\tau_0=10\,\tau_1$, as in some actual experiments.

We note that the Ramsey fringe patterns are in general not symmetric with respect to the substitution $\eta\to-\eta$. Symmetry is obtained only for $\chi=\pm\pi/2$, *i.e.*, $\cos\chi=0$, maximal asymmetry for $\chi=0$ and $\chi=\pm\pi$, *i.e.*, $\sin\chi=0$. At first sight the whole fringe pattern appears to be shifted from the exact resonance frequency ω_c toward the left or toward the right, depending on the phase χ. It is therefore not immediately obvious how to identify the Ramsey fringe belonging to the exact resonance frequency ω_c without knowing the value

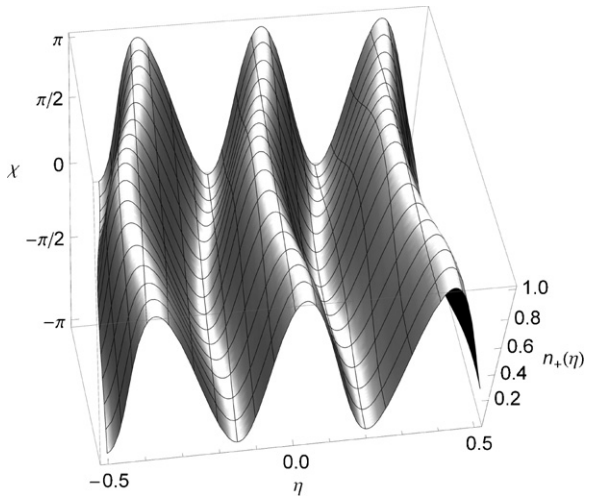

Fig. 8. Three fringes nearest to the resonance position $\eta=0$, for 2-pulse Ramsey excitation. The central peak coincides with the exact resonance position, marked by the heavy black line, only for phase $\chi=\pm\pi/2$, otherwise small shifts of the peak values toward both sides are observed. The figure shows a plot of the surface $n_+(\theta_0=5, \theta_1=0.5, \eta, \chi)$, assuming $R_+(0)\approx0.25\,R_-(0)$.

of the phase χ. A closer inspection shows, however, that with varying χ the envelope of the whole fringe pattern changes, while the individual fringes stay more or less at their place. In other words, we see a change of the maximum values of the fringes with varying χ in conjunction with minute changes of the fringe positions. This is further illustrated in Fig. 8 which shows a 3D-plot of the surface $n_+(\theta_0=5, \theta_1=0.5, \eta, \chi)$. As in the case of conventional one-pulse excitation, the peak value of the fringe at the resonance position occurs at $\eta=0$ only for $\chi=\pm\pi/2$, otherwise small deviations are observed. A comparison with Fig. 4 shows that for Ramsey fringes the shift is on a smaller scale than for one-pulse excitation.

Let us now combine all conversion profiles for $-\pi\le\chi\le+\pi$ into a single plot, corresponding to the projection of Fig. 8 along the χ-axis onto the (η, n_+)-plane. Then the conversion profiles shall fill the shaded regions in Fig. 9. Therefore, with a random choice of the phase χ the theory predicts data points obtained in an experiment to lie not on a mathematical curve, but within a band with a finite width, which is determined by the component of cyclotron motion that was present in the initial state. Thus we may expect experimentally observed Ramsey fringes to have a fuzzy and

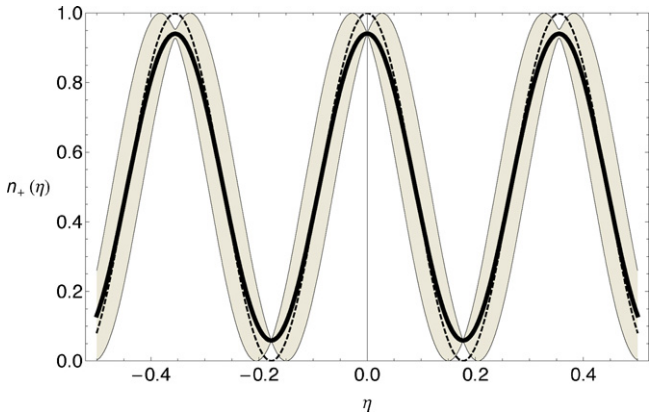

Fig. 9. The conversion profiles for fixed phase χ as plotted in Fig. 7 fill the shaded region. The width of this band is proportional to the initial radius of the cyclotron motion $R_+(0)$. This figure assumes $R_+(0)\approx0.25R_-(0)$. The heavy black curve is the phase-averaged Ramsey profile. The dashed line represents the Ramsey profile calculated with the assumption that initially the ions are in a pure magnetron state, *i.e.*, $R_+(0)=0$.

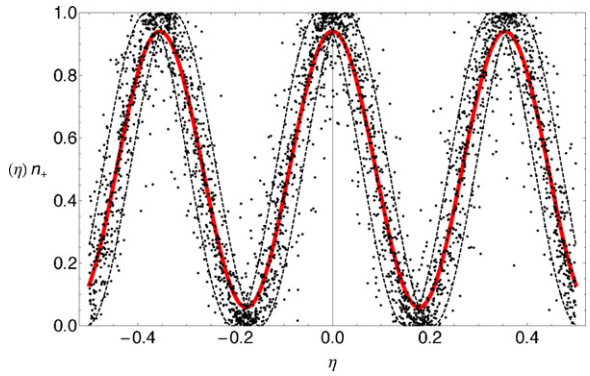

Fig. 10. Simulation of the data obtained from 3000 single ions, assuming a random distribution of the phase χ and a Gaussian distribution for the initial values of the cyclotron radius $R_+(0)$, with variance $\sqrt{\langle R_+(0)^2\rangle} = 0.25\,R_-(0)$. The solid curve is the phase-averaged Ramsey profile for $R_+(0) = 0.25\,R_-(0)$, Eq. (41). The two dashed lines define the band into which all data points with $R_+(0) < 0.25\,R_-(0)$ are expected to fall.

diffuse appearance when a sizeable component of cyclotron motion was present in the initial state. Next we average over the phase χ. From Eq. (38) we obtain the phase-averaged Ramsey profile as

$$\overline{n}_+(\theta_0, \theta_1, \eta) = \left|\mathcal{R}'_{11}\right|^2 n_{0+} + \left|\mathcal{R}'_{12}\right|^2 n_{0-} = n_{0+} + \left|\mathcal{R}'_{12}(\theta_0, \theta_1, \eta)\right|^2 (1 - 2\,n_{0+}). \quad (41)$$

In the last step we have used the unitarity of the Ramsey matrix $\left|\mathcal{R}'_{11}\right|^2 + \left|\mathcal{R}'_{12}\right|^2 = 1$ and $n_{0-} = 1 - n_{0+}$. Eq. (41) is a slight generalization of the well known formula (40) containing the additional parameter n_{0+}. The phase-averaged Ramsey profile is shown in Fig. 9 as the thick black curve within the shaded region. For comparison the profile expected for an initial state with pure magnetron motion is also shown as a thin dashed line.

In the same way as for 1-pulse excitation one can simulate the expected outcome of a Ramsey type measurement, assuming a random distribution of the phases and a Gaussian distribution of the initial values of the cyclotron radius. Fig. 10 shows our result for a sample of 3000 ions, assuming for the variance of the Gaussian distribution $\sqrt{\langle R_+(0)^2\rangle} = \kappa\,R_-(0)$ with $\kappa = 0.25$. The solid line represents the phase-averaged Ramsey profile calculated from Eq. (41), and the dashed lines mark the boundaries of the band into which data points are expected to fall, when the initial cyclotron radius is $R_+(0) < 0.25\,R_-(0)$. The distribution of the data points over a band of finite width causes a fuzzy appearance of the Ramsey profile, with accumulations near the maxima and minima of the Ramsey profile. These accumulations are due to cyclotron radii $R_+(0) \ll \kappa\,R_-(0)$, which have high weight in the assumed Gaussian distribution of $R_+(0)$.

Several publications by the JYFLTRAP-collaboration have presented experimental data plots that show the features just described, a wide scatter of the experimental data points about the average curve representing the Ramsey fringes and accumulations near the extrema of the Ramsey profile (Fig. 1 in [30], Fig. 2 in [31], Fig. 2 in [32], and others).

The number of ions available for one experiment is often much smaller than assumed for Figs. 6 and 10. We therefore compare in Fig. 11 four simulations: for a large number (1500) and a small number (150) of ions, and for very small ($\kappa = 0.01$) and for rather large ($\kappa = 0.25$) initial cyclotron radii. When the assumed

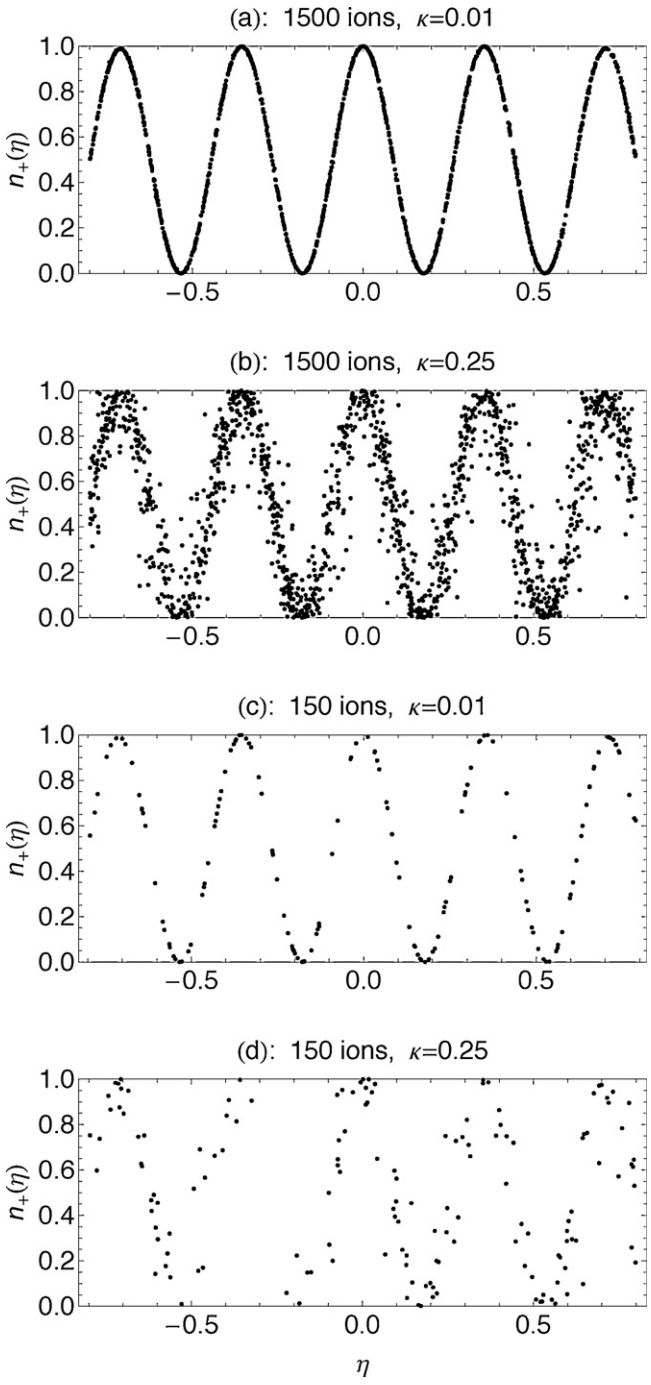

Fig. 11. Dependence of simulated Ramsey profiles on the number of ions and on the initial cyclotron radius. All graphs assume a random distribution of the phases χ and a Gaussian distribution of the initial values of the cyclotron radius $R_+(0)$ with variance $\sqrt{\langle R_+(0)^2\rangle} = \kappa\,R_-(0)$. The definition of the Ramsey profiles is much better for a sample with a large number (1500) of single ions than for one with a small number (150). A wide distribution of the initial cyclotron radii causes fuzzy profiles (b), or for small ion numbers, makes the profiles barely recognizable (d).

Gaussian distribution with variance $\sqrt{\langle R_+(0)^2\rangle} = \kappa\,R_-(0)$ is very narrow ($\kappa = 0.01$) the Ramsey profiles are well defined even for small ion numbers (Fig. 11c). On the other hand, for a wide distribution of initial cyclotron radii ($\kappa = 0.25$) the profiles are quite fuzzy even for large ion numbers (Fig. 11b), and they are rather ill defined for small ion numbers (Fig. 11d).

6. Conclusions

In this paper we have studied the resonant interconversion of the radial motional modes in a Penning trap by one or two pulses of an external quadrupolar rf-field, which is part of the mass spectrometric measurement cycle. Ideally ions are prepared in a state of pure magnetron motion, which is then converted into cyclotron motion. In real experiments, however, the initial motional states that one can prepare are predominantly magnetron motion, but they always contain a remaining small component of cyclotron motion which is unknown or only poorly known. Our interest here centered on the relevance of this fact for the evaluation of experiments. We have studied in detail conventional one-pulse quadrupolar excitation as well as two-pulse Ramsey excitation.

We have shown that a non-vanishing component of cyclotron motion induces phase-dependent phenomena, such as asymmetric conversion profiles, shifts of conversion maxima and minima, modified conversion times and so on. The phases of the cyclotron and of the magnetron oscillators, χ_+ and χ_-, and the phase χ_q of the quadrupolar rf-field always enter in the combination $\chi = \chi_q - \chi_+ - \chi_-$. Most experiments do not have control over the phase χ, because they cannot control the phase χ_+ of the cyclotron oscillator. Therefore, in most experiments the measured conversion line shapes, excitation curves, and conversion times are averages over the uniform distribution of the phase χ and over the probability distribution of the initial radii $R_+(0)$. The latter depends on the method by which the ions were placed in the trap.

Phase-dependent shifts of the conversion maxima and minima cancel out when we average over the phase χ. Therefore phase-averaged conversion line shapes have their maxima and minima at exactly the same frequencies as conversion profiles obtained with an initial state of pure magnetron motion. Thus the precise determination of the resonance frequency ω_c for mass spectrometric purposes is not affected. On the other hand, experimental data points are expected to lie not on a mathematical curve, as for an initial state of pure magnetron motion, but within a band of finite width about the phase-averaged curve. The width of the band is the larger, the larger the initial cyclotron radius $R_+(0)$ is. Both facts together explain why experimental data sets often have a fuzzy and diffuse appearance.

In summary, what have we learnt for the design of experiments? (a) Most importantly, the cyclotron frequency ω_c determined from a data set with a random phase distribution is the same as that expected in the ideal case (all ions initially in a state of pure magnetron motion). Therefore mass determinations are not adversely affected by the lack of knowledge of the phase χ. (b) In the ideal case (initially pure magnetron motion) resonance curves are sharply defined. Under real conditions (the initial motional state of the ions contains a cyclotron component) the resonance curve is smeared into a band with a finite width depending on the size of the cyclotron component in the initial state. There is still no shift of the resonance position, but the resonance curve becomes fuzzy. For high statistics experiments this may still be tolerable, however for low statistics the ensuing lack of definition of the resonance signal may become a problem. Our results underscore that a careful preparation of the initial magnetron state of motion of the ions is important for the quality of the experimental data. Cooling the initial component of cyclotron motion to a minimal value is rewarded with sharp conversion profiles for conventional one-pulse and for two-pulse Ramsey excitation. (c) The strength of the expected initial cyclotron component provides a new parameter n_{0+} that may be used in data fitting.

References

[1] K. Blaum, Phys. Rep. 425 (2006) 1.
[2] L. Schweikhard, G. Bollen (Eds.), Int. J. Mass Spectrom. 251 (2006) (special issue).
[3] L.S. Brown, G. Gabrielse, Rev. Mod. Phys. 58 (1986) 233.
[4] P.K. Ghosh, in: Ion Traps, Clarendon Press, Oxford, 1995.
[5] F.G. Major, V.N. Gheorghe, G. Werth, in: Charged Particle Traps, Physics and Techniques of Charged Particle Field Confinement (Springer Series on Atomic, Optical, and Plasma Physics, Vol. 37), Springer-Verlag, Berlin, 2005.
[6] G. Bollen, R.B. Moore, G. Savard, H. Stolzenberg, J. Appl. Phys. 68 (1990) 4355.
[7] K. Blaum, F. Herfurth, A. Kellerbauer, H.-J. Kluge, M. Kuckein, S. Heinz, P. Schmidt, L. Schweikhard, J. Phys. B: Atom. Mol. Opt. Phys. 36 (2003) 921.
[8] R. Ringle, G. Bollen, A. Prinke, J. Savory, P. Schury, S. Schwarz, T. Sun, Int. J. Mass Spectrom. 263 (2007) 38–44.
[9] H. Stolzenberg, St. Becker, G. Bollen, F. Kern, H.-J. Kluge, T. Otto, G. Savard, L. Schweikhard, G. Audi, R.B. Moore, Phys. Rev. Lett. 65 (1990) 3104.
[10] G. Savard, St. Becker, G. Bollen, H.-J. KLuge, R.B. Moore, T. Otto, L. Schweikhard, H. Stolzenberg, U. Wiess, Phys. Lett. A 158 (1991) 247.
[11] G. Gräff, H. Kalinowsky, J. Traut, Z. Phys. A 297 (1980) 35.
[12] K. Blaum, Sz. Nagy, G. Werth, J. Phys. B: Atom. Mol. Opt. Phys. 42 (2009) 154015.
[13] L. Schweikhard, A.G. Marshall, J. Am. Soc. Mass Spectrom. 4 (1993) 433.
[14] R. Ringle, G. Bollen, P. Schury, S. Schwarz, T. Sun, Int. J. Mass Spectrom. 262 (2007) 33.
[15] M. Kretzschmar, Trapped Charged Particles and Fundamental Physics, in: D.H.E. Dubin, D. Schneider (Eds.), in: AIP Conf. Proc., vol. 457, The American Institute of Physics, 1999, pp. 242–251.
[16] M.O. Scully, M.S. Zubairy, in: Quantum Optics, Cambridge University Press, 1997.
[17] S. Eliseev, M. Block, A. Chaudhuri, F. Herfurth, H.-J. Kluge, A. Martin, C. Rauth, G. Vorobjev, Int. J. Mass Spectrom. 262 (2007) 45.
[18] M. König, G. Bollen, H.-J. Kluge, T. Otto, J. Szerypo, Int. J. Mass Spectrom. Ion Process. 142 (1995) 95.
[19] M. Kretzschmar, Int. J. Mass Spectrom. 264 (2007) 122.
[20] N.F. Ramsey, Phys. Rev. 76 (1949) 996, Phys. Rev. 78 (1950) 695, and Rev. Mod. Phys. 62 (1990) 541.
[21] G. Bollen, H.-J. Kluge, T. Otto, G. Savard, H. Stolzenberg, Nucl. Instrum. Methods B 70 (1992) 490.
[22] S. George, K. Blaum, F. Herfurth, A. Herlert, M. Kretzschmar, S. Nagy, S. Schwarz, L. Schweikhard, C. Yazidjian, Int. J. Mass Spectrom. 264 (2007) 110.
[23] S. George, S. Baruah, B. Blank, K. Blaum, M. Breitenfeldt, U. Hager, F. Herfurth, A. Herlert, A. Kellerbauer, H.-J. Kluge, M. Kretzschmar, D. Lunney, R. Savreux, S. Schwarz, L. Schweikhard, C. Yazidjian, Phys. Rev. Lett. 98 (2007) 162501.
[24] S. George, G. Audi, B. Blank, K. Blaum, M. Breitenfeldt, U. Hager, F. Herfurth, A. Herlert, A. Kellerbauer, H.-J. Kluge, M. Kretzschmar, D. Lunney, R. Savreux, S. Schwarz, L. Schweikhard, C. Yazidjian, Eur. Phys. Lett. 82 (2008) 50005.
[25] J. Ketelaer, T. Beyer, K. Blaum, M. Block, K. Eberhardt, M. Eibach, F. Herfurth, C. Smorra, Sz. Nagy, Eur. Phys. J. D 58 (2010) 47.
[26] M. Mukherjee, D. Beck, K. Blaum, G. Bollen, J. Dilling, S. George, F. Herfurth, A. Herlert, A. Kellerbauer, H.-J. Kluge, S. Schwarz, L. Schweikhard, C. Yazidjian, Eur. Phys. J. A 35 (2008) 1.
[27] M. Kowalska, for the ISOLTRAP collaboration, Hyperfine Interact. 196 (2010) 199.
[28] V.-V. Elomaa, T. Eronen, J. Hakala, A. Jokinen, A. Kankainen, I.D. Moore, S. Rahaman, J. Rissanen, C. Weber, J. Äystö, Nucl. Instrum. Methods Phys. Res. A 612 (2009) 97.
[29] N.D. Scielco, S. Caldwell, G. Savard, J.A. Clark, C.M. Deibel, J. Fallis, S. Gulick, D. Lascar, A.F. Levand, G. Li, J. Mintz, E.B. Norman, K.S. Sharma, M. Sternberg, T. Sun, J. van Schelt, Phys. Rev. C 80 (2009) 025501.
[30] T. Eronen, V.-V. Elomaa, J. Hakala, J.C. Hardy, A. Jokinen, I.D. Moore, M. Reponen, J. Rissanen, A. Saastamoinen, C. Weber, J. Äystö, Phys. Rev. Lett. 103 (2009) 252501.
[31] S. Rahaman, V.-V. Elomaa, J. Hakala, T. Eronen, A. Jokinen, A. Kankainen, J. Rissanen, J. Suhonen, C. Weber, J. Äystö, Phys. Rev. Lett. 103 (2009) 042501.
[32] V.S. Kolhinen, T. Eronen, D. Gorelov, J. Hakala, A. Jokinen, A. Kankainen, I.D. Moore, J. Rissanen, A. Saastamoinen, J. Suhonen, J. Äystö, Phys. Rev. C 82 (2010) 022501(R).